A switched adaptive observer for extended braking stiffness estimation

Missie Aguado-Rojas William Pasillas-Lépine
Antonio Loría

Laboratoire des Signaux et Systèmes (L2S)

Journée d'observation 9/02/2018

Motivation

“Safety is a basic tenet to the [automotive] industry now and will continue to be an ongoing major focus for consumers and manufacturers alike.”

Outline

Part I Extended braking stiffness estimation

- Introduction
- XBS dynamics
- Switched adaptive observer
- Simulation and experimental results

Part II Wheel angular velocity and acceleration estimation

- Introduction
- Problem description
- Measurement models
- Estimation algorithm
- Experimental results

Part I

Extended braking stiffness estimation

Wheel dynamics

The longitudinal dynamics of the angular velocity ω of the wheel is described by

Wheel dynamics

The longitudinal dynamics of the angular velocity ω of the wheel is described by

$$I\dot{\omega} = -RF_x - \gamma_b P_b$$

$$F_x = \mu(\lambda) F_z$$

$$\lambda = \frac{R\omega - v_x}{v_x}$$

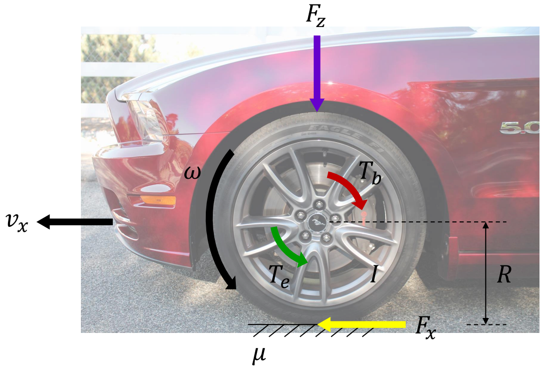

where I is the inertia of the wheel, R is its effective rolling radius, γ_b is the brake efficiency, P_b is the brake pressure, F_x is the tyre force, F_z is the vertical load, $\mu(\lambda)$ is the tyre-road friction coefficient, λ is the wheel slip, and v_x is the speed of the vehicle.

Tyre-road friction coefficient

Burckhardt's tyre characteristic model is defined as

$$\mu(\lambda) = c_1(1 - \exp(-c_2\lambda)) - c_3\lambda$$

where the constants c_i depend on the road conditions.

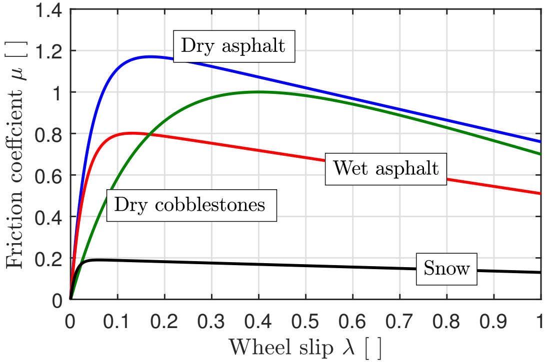

Figure: *Typical tyre-road friction curve for different road surface conditions.*

Extended braking stiffness (XBS)

The XBS is defined as the slope of friction coefficient against wheel slip at the operating point, i.e.

$$\frac{d\mu(\lambda)}{d\lambda} = c_1 c_2 \exp(-c_2\lambda)) - c_3.$$

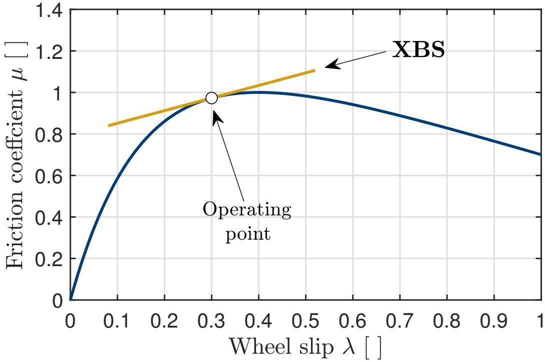

Figure: *Tyre-road friction and extended braking stiffness (XBS).*

State-of-the-art on XBS estimation

- [Sugai et al., 1999] Analysis of the frequency characteristics of a resonance system composed of the vehicle body, the wheel and the road surface.
- [Umeno, 2002] Instrumental variable method. Linearization around a constant-velocity operating point.
- [Ono et al., 2003] Recursive least squares algorithm. The XBS is (implicitly) assumed constant.
- [Villagra et al., 2011] Elementary diagnostic tools and algebraic methods to distinguish one type of road from another. The estimation results are accurate only within a certain validity range.
- [Hoàng et al., 2013; 2014] Augmented-state observer. Requires (some) knowledge about the road conditions.

Wheel acceleration and XBS dynamics

Defining as state variables $z_1 = R\dot{\omega} - \dot{v}_x$ and $z_2 = \frac{\mathrm{d}\mu(\lambda)}{\mathrm{d}\lambda}$, we obtain

$$\dot{z}_1 = -\frac{a}{v_x(t)} z_1 z_2 - bu \tag{1a}$$

$$\dot{z}_2 = (cz_2 + d)\frac{1}{v_x(t)} z_1 \tag{1b}$$

where $a = \frac{R^2}{I} F_z$, $b = \frac{R}{I}\gamma_b$ are known constant parameters, $u = \dot{P}_b$, $c = -c_2$, $d = -c_2 c_3$ are unknown parameters that depend on the road conditions, and v_x is considered as a known external variable.

The **objective** is to design an observer to estimate the (unmeasurable) XBS z_2 under unknown road conditions, using the available information of the wheel acceleration offset z_1.

Change of coordinates

In order for the system to have a convenient structure that allows us to exploit well-known tools available in the literature, we propose the linear change of coordinates

$$
\begin{aligned}
w_1 &= z_1 \\
w_2 &= z_2 + \frac{c}{a} z_1
\end{aligned}
$$

which transforms system (1) into

$$
\begin{aligned}
\dot{w}_1 &= \frac{w_1}{v_x(t)}(c w_1 - a w_2) - b u \\
\dot{w}_2 &= -\frac{bc}{a} u + \frac{w_1}{v_x(t)} d
\end{aligned}
$$

Change of coordinates

or, equivalently,

$$\dot{w}(t) = A(t,y)w(t) + Bu(t) + \Psi(t,u,y)\theta \tag{2a}$$
$$y(t) = Cw(t) \tag{2b}$$

with

$$A(t,y) = \frac{w_1}{v_x(t)}\begin{pmatrix} 0 & -a \\ 0 & 0 \end{pmatrix}, \qquad \Psi(t,u,y) = \begin{pmatrix} \frac{w_1^2}{v_x(t)} & 0 \\ -\frac{b}{a}u & \frac{w_1}{v_x(t)} \end{pmatrix}$$

$$B = \begin{pmatrix} -b \\ 0 \end{pmatrix}, \quad C = \begin{pmatrix} 1 & 0 \end{pmatrix}, \quad \theta = \begin{pmatrix} c \\ d \end{pmatrix}, \quad w = \begin{pmatrix} w_1 \\ w_2 \end{pmatrix}.$$

XBS observer

Based on the adaptive observer proposed in [Zhang, 2002], and following ideas presented in [Hoàng et al., 2013; 2014], we propose

$$\begin{aligned} \dot{\hat{w}}(t) &= A(t,y)\hat{w}(t) + Bu(t) + \Psi(t,u,y)\hat{\theta}(t) \\ &\qquad + \left(K(t,y) + \Upsilon(t)\Gamma\Upsilon^\top(t)C^\top\right)\left(y(t) - C\hat{w}(t)\right) \quad (3a) \\ \dot{\hat{\theta}}(t) &= \Gamma\Upsilon^\top(t)C^\top\left(y(t) - C\hat{w}(t)\right) \quad (3b) \\ \dot{\Upsilon}(t) &= \left(A(t,y) - K(t,y)C\right)\Upsilon(t) + \Psi(t,u,y) \quad (3c) \end{aligned}$$

with $\Gamma = \Gamma^\top > 0$ and

$$K(t,y) = \frac{w_1}{v_x(t)} \times \begin{cases} \begin{pmatrix} k_1^+ \\ k_2^+ \end{pmatrix}, & \text{if } y = w_1 > 0 \\ \begin{pmatrix} k_1^- \\ k_2^- \end{pmatrix}, & \text{if } y = w_1 < 0 \end{cases} \quad (4)$$

XBS observer

Theorem 1

Consider system (2) and observer (3). Define $\tilde{w} = \hat{w} - w$ *and* $\tilde{\theta} = \hat{\theta} - \theta$. *Let the observer gains* $k_{1,2}^{\pm}$ *in (4) satisfy*

$$k_1^+ > 0, \qquad k_2^+ < 0, \qquad k_1^- = -k_1^+ < 0, \qquad k_2^- = k_2^+ < 0.$$

Assume that the switching signal $\sigma(w_1)$ *that selects the observer gains admits a strictly positive minimal dwell time, that is, any two consecutive switchings are separated by no less than* $\tau_D > 0$. *If* $\Psi(t, u(t), y(t))$ *is persistently exciting, then the origin of the closed-loop system with state* $(\tilde{w}, \tilde{\theta})^\top$ *is globally asymptotically stable.*

Dwell time and PE during ABS braking

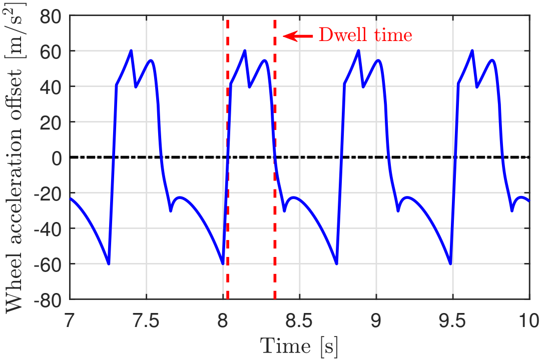

Figure: *Measured output w_1 during an ABS braking simulation.*

Dwell time and PE during ABS braking

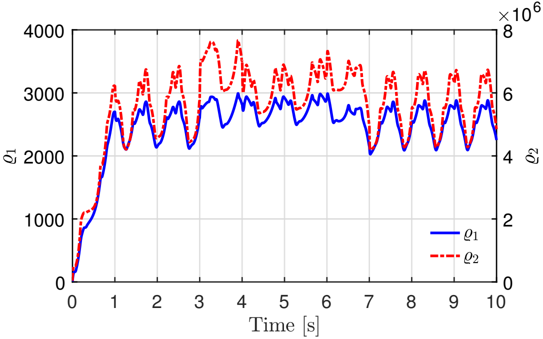

Figure: *Eigenvalues of* $M(t) = \int_{t-T}^{t} \Psi(\tau, u(\tau), y(\tau))^\top \Psi(\tau, u(\tau), y(\tau)) d\tau$ *during an ABS braking simulation.*

Simulation results

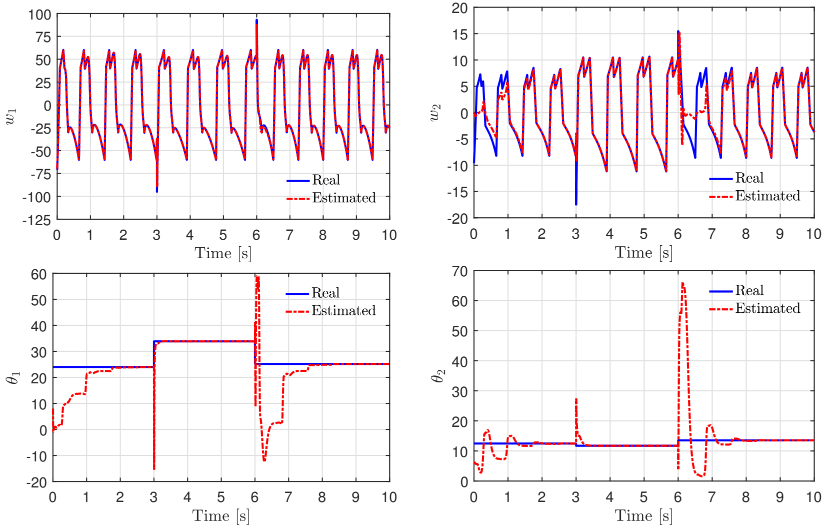

Figure: *Real vs estimated states and parameters of the transformed system.*

Inverse change of coordinates

The states of the original system are obtained with

$$\hat{z}_1 = \hat{w}_1$$
$$\hat{z}_2 = \hat{w}_2 - \frac{\hat{c}}{a}\hat{w}_1.$$

Since $\tilde{w} \to 0$ and $\tilde{\theta} \to 0$, then $\tilde{z} = \hat{z} - z \to 0$.

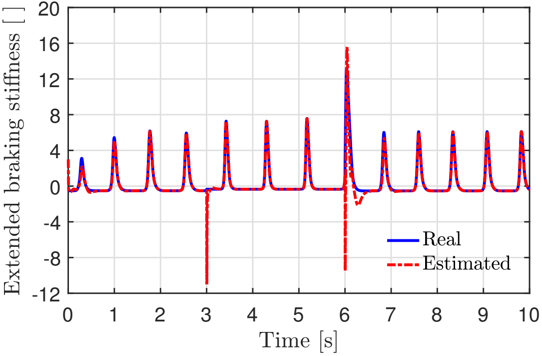

Figure: *Real vs estimated XBS (simulation results).*

Experimental setup (TU Delft)

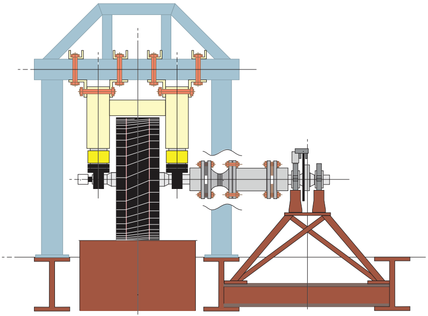

Figure: *Tyre-in-the-loop testbench.*

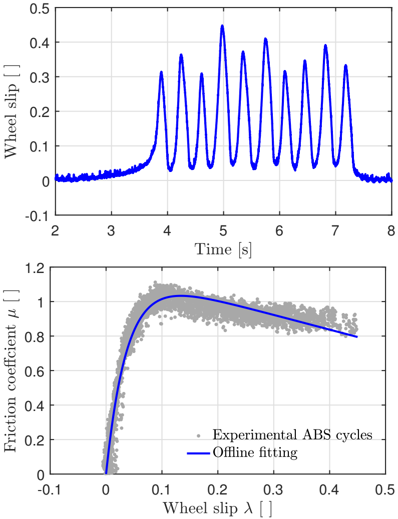

Figure: *ABS regulation test.*

Experimental results

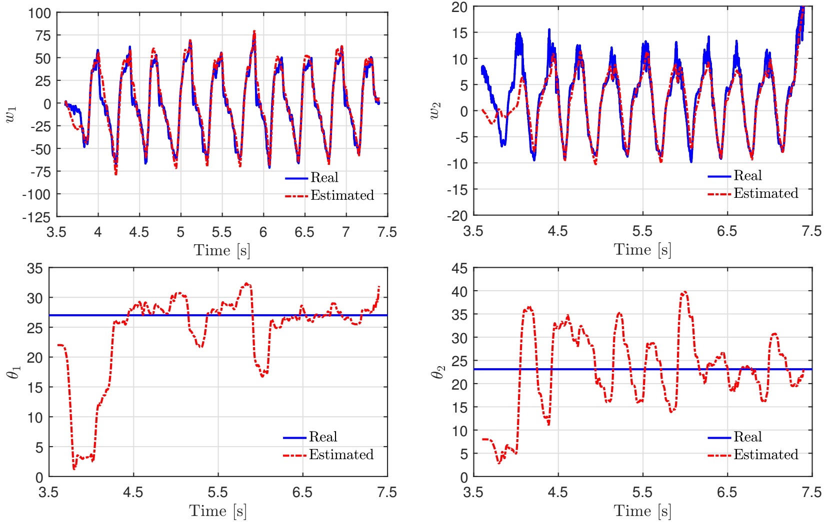

Figure: *Real vs estimated states and parameters of the transformed system.*

Experimental results

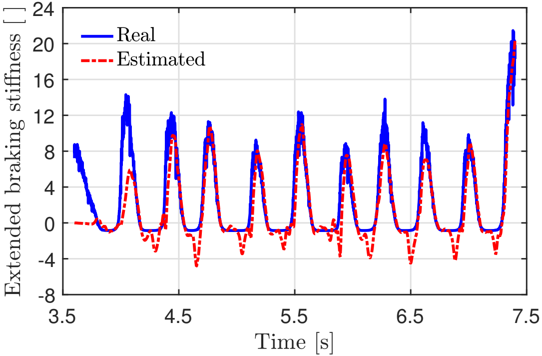

Figure: *Real vs estimated XBS.*

Experimental results

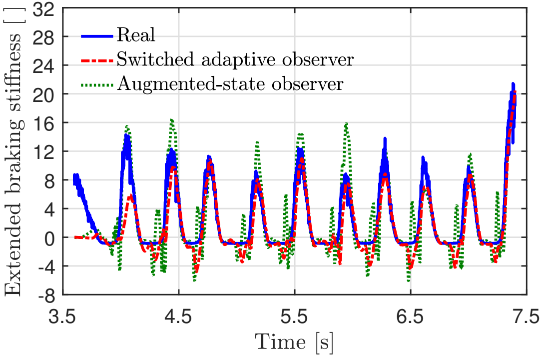

Figure: *Comparison against augmented-state observer.*

Experimental results

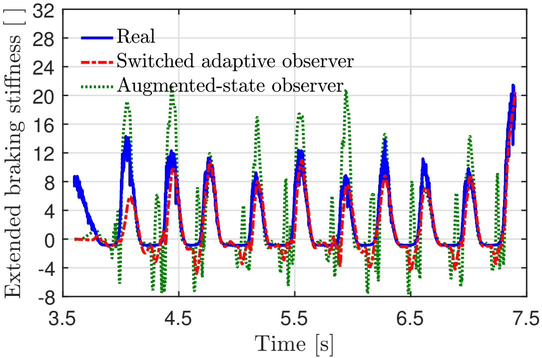

Figure: *Comparison against augmented-state observer.*

Experimental results

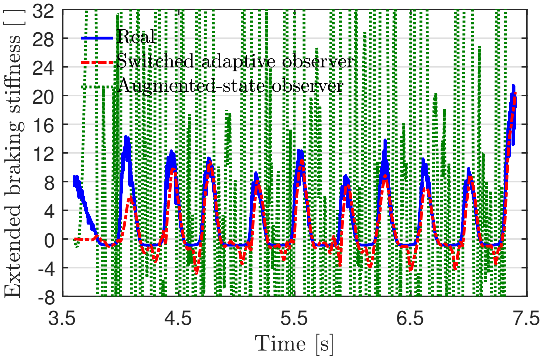

Figure: *Comparison against augmented-state observer.*

Simulation results: with perturbed measurements

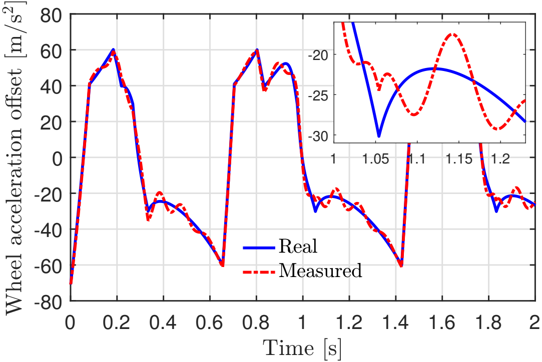

Figure: *Wheel acceleration offset: real signal vs perturbed measurement.*

Simulation results: with perturbed measurements

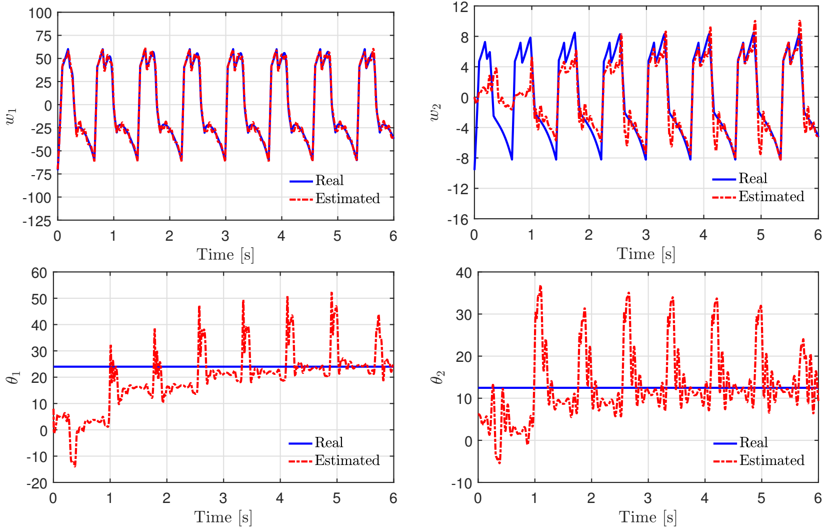

Figure: *Real vs estimated states and parameters of the transformed system.*

Simulation results: with perturbed measurements

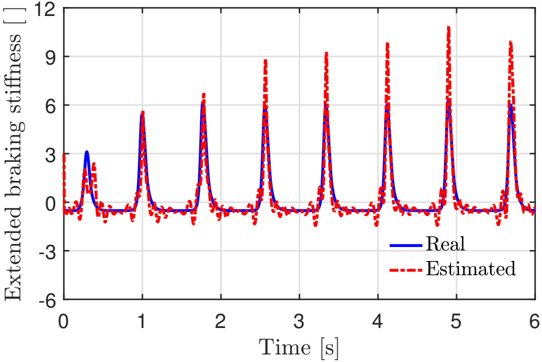

Figure: *Real vs estimated XBS.*

Part II

Wheel angular velocity and acceleration estimation

Wheel velocity estimation mechanism

The most commonly used technology to measure rotational velocity is based on incremental shaft encoders.

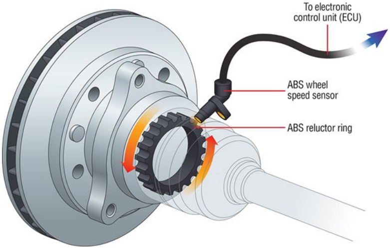

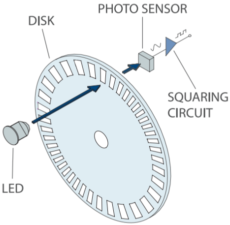

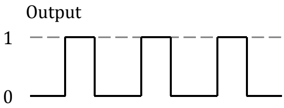

Time-stamping algorithm [Merry et al., 2010; 2013]

It consists in capturing the time instants t_i and positions θ_i of the last n encoder events, and performing an m-th-order polynomial fit to approximate the position of the wheel.

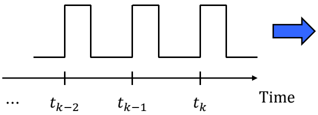

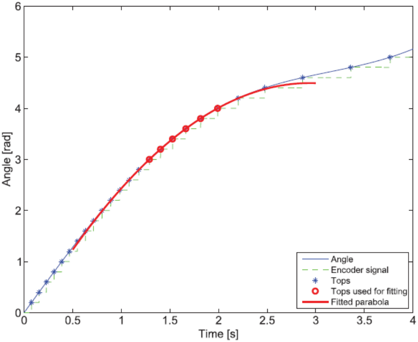

Time-stamping algorithm [Merry et al., 2010; 2013]

The position at time $t = t_k$ is approximated by

$$\theta(t) = p_m t^m + p_{m-1} t^{m-1} + \ldots + p_0.$$

The regression problem

$$\begin{pmatrix} t_{k-n+1}^m & t_{k-n+1}^{m-1} & \cdots & t_{k-n+1} & 1 \\ \vdots & \vdots & \vdots & \vdots & \vdots \\ t_k^m & t_k^{m-1} & \cdots & t_k & 1 \end{pmatrix} \begin{pmatrix} p_m \\ \vdots \\ p_0 \end{pmatrix} = \begin{pmatrix} \theta_{k-n+1} \\ \vdots \\ \theta_k \end{pmatrix}$$

is solved for p_i via the least squares method, and the velocity and acceleration are calculated with

$$\omega(t) = \sum_{i=1}^m i p_i t^{i-1}, \qquad \alpha(t) = \sum_{i=2}^m (i-1) i p_i t^{i-2}.$$

Encoder imperfections

An ideal encoder is characterised by identical and equidistant teeth distributed over the encoder's code-wheel. However, in real devices sensor imperfections inevitably occur:

Encoder imperfections

An ideal encoder is characterised by identical and equidistant teeth distributed over the encoder's code-wheel. However, in real devices sensor imperfections inevitably occur:

- Cycle error

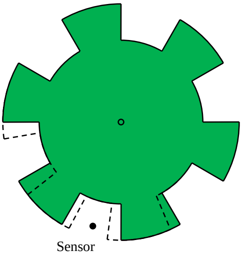

Encoder imperfections

An ideal encoder is characterised by identical and equidistant teeth distributed over the encoder's code-wheel. However, in real devices sensor imperfections inevitably occur:

- Cycle error
- Eccentricity or tilt of the encoder's code-wheel

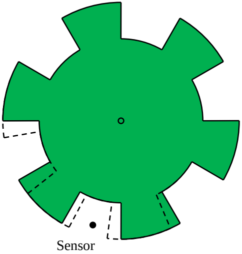

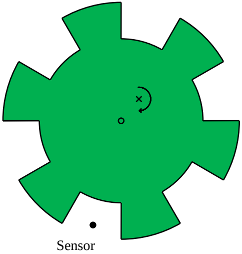

Encoder imperfections

An ideal encoder is characterised by identical and equidistant teeth distributed over the encoder's code-wheel. However, in real devices sensor imperfections inevitably occur:

- Cycle error
- Eccentricity or tilt of the encoder's code-wheel
- Pulse-width and phase errors

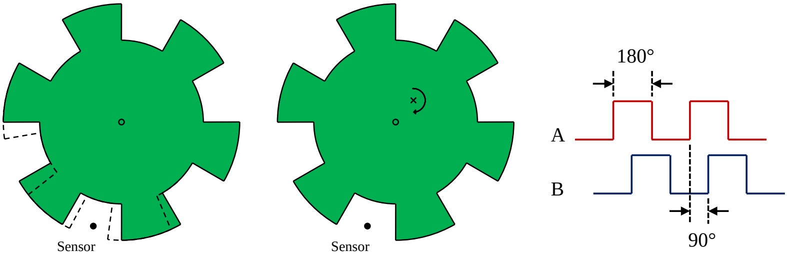

Effects of encoder imperfections

In the presence of sensor imperfections, the measured position

$$\theta_m = \theta_r + f_r(\theta_r)$$

is affected by a small perturbation that *may* be neglected.

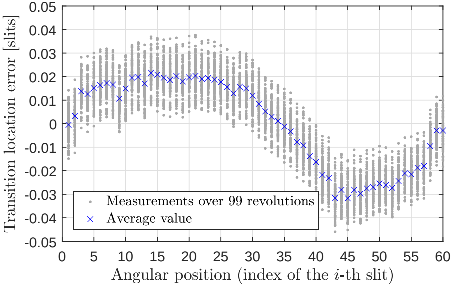

Figure: *Error in pulse transition location as a function of angular position for a 60 pulses-per-revolution encoder.*

Effects of sensor imperfections

In the case of the measured velocity and acceleration

$$\omega_m = \omega_r + \omega_r f_r'(\theta_r)$$

$$\alpha_m = \alpha_r + \alpha_r f_r'(\theta_r) + \omega_r^2 f_r''(\theta_r)$$

the perturbation cannot be neglected.

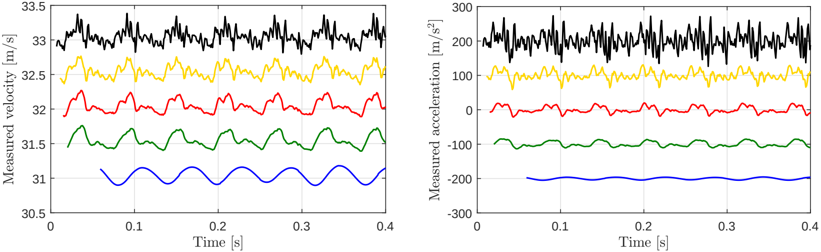

Figure: *Velocity and acceleration measured via the time-stamping algorithm for a 32 m/s constant-velocity reference using different numbers of events.*

State-of-the-art

- [Merry et al., 2013] Error compensation look-up tables. They work only for a particular encoder and their construction requires a high-resolution reference sensor.
- [Gustafsson, 2010] Frequency analysis of the wheel speed for the estimation of the encoder imperfections. Works only when the speed is constant.
- [Corno and Savaresi, 2010] Notch filter.
- [Panzani et al., 2012] Notch filter.
- [Hoàng et al., 2012] Notch filter.
- [Rallo et al., 2017] Batch constrained least squares algorithm for the estimation of the encoder imperfections. Assumes that the speed does not vary significantly within a single revolution.

Measurement models

In order to estimate ω_r and α_r from the available signals, we introduce the measurement models:

- $$\theta_m = \theta_r + \sum_{k=1}^{M} \left[a_k \sin(k\theta_m) + b_k \cos(k\theta_m)\right]$$
- $$\omega_m = \omega_r + \omega_m \sum_{k=1}^{M} \left[k a'_k \cos(k\theta_m) - k b'_k \sin(k\theta_m)\right]$$
- $$\begin{aligned}\alpha_m = \alpha_r &+ \alpha_m \sum_{k=1}^{M} \left[k a''_k \cos(k\theta_m) - k b''_k \sin(k\theta_m)\right] \\ &- \omega_m^2 \sum_{k=1}^{M} \left[k^2 a''_k \sin(k\theta_m) + k^2 b''_k \cos(k\theta_m)\right]\end{aligned}$$

where a_k, b_k, a'_k, b'_k, a''_k and b''_k are unknown.

Measurement models

In order to estimate ω_r and α_r from the available signals, we introduce the measurement models:

- $$\theta_m = \theta_r + \sum_{k=1}^{M} \left[a_k \sin(k\theta_m) + b_k \cos(k\theta_m)\right]$$
- $$\omega_m = \omega_r + \omega_m \sum_{k=1}^{M} \left[k a'_k \cos(k\theta_m) - k b'_k \sin(k\theta_m)\right]$$
- $$\begin{aligned}\alpha_m = \alpha_r &+ \alpha_m \sum_{k=1}^{M} \left[k a''_k \cos(k\theta_m) - k b''_k \sin(k\theta_m)\right] \\ &-\omega_m^2 \sum_{k=1}^{M} \left[k^2 a''_k \sin(k\theta_m) + k^2 b''_k \cos(k\theta_m)\right]\end{aligned}$$

where a_k, b_k, a'_k, b'_k, a''_k and b''_k are unknown.

⚠ In general, $a_k \neq a'_k \neq a''_k$ and $b_k \neq b'_k \neq b''_k$. ⚠

Measurement models

⚠ Due to the delay introduced in the measured signals by the time-stamping algorithm, in general, $a_k \neq a'_k \neq a''_k$ and $b_k \neq b'_k \neq b''_k$. ⚠

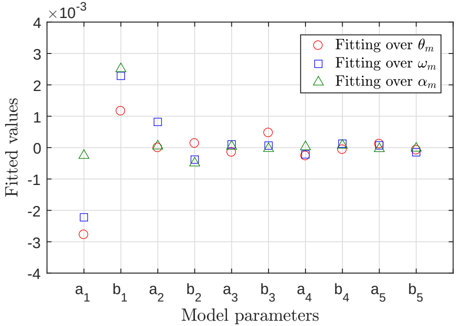

Figure: *Off-line least-squares fitting of the Fourier coefficients a_k and b_k for the measurement models.*

Estimation algorithm

Let us rewrite the measurement models as:

$$\omega_m = \omega_r + \omega_m \phi(\theta_m)^\top D \vartheta' \tag{5}$$

$$\alpha_m = \alpha_r + \left[\alpha_m \phi(\theta_m)^\top D - \omega_m^2 \psi(\theta_m)^\top D^2\right] \vartheta'' \tag{6}$$

where

$$D = \operatorname{diag}(1, 1, 2, 2, \ldots)$$

$$\phi(\theta_m) = \begin{bmatrix} \cos(\theta_m) & -\sin(\theta_m) & \cos(2\theta_m) & -\sin(2\theta_m) & \cdots \end{bmatrix}^\top$$

$$\psi(\theta_m) = \begin{bmatrix} \sin(\theta_m) & \cos(\theta_m) & \sin(2\theta_m) & \cos(2\theta_m) & \cdots \end{bmatrix}^\top$$

and ϑ', ϑ'' contain the corresponding coefficients a'_k, b'_k, a''_k, b''_k.

Estimation algorithm

From (5) and (6), ω_m and α_m can be seen as the sum of a low-frequency term and a high-frequency (with respect to the first one) term, of the form

$$\bar{\zeta} = \Phi(\theta_m, \omega_m, \alpha_m)^\top \vartheta. \tag{7}$$

that depends on the known signals θ_m, ω_m, and α_m, and is linear in the unknown parameters ϑ.

In order to estimate ω_r and α_r we propose:

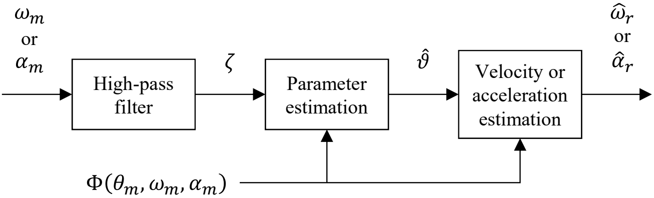

Estimation algorithm

Stage 1: The measured signals are filtered in order to separate the perturbation term $\bar{\zeta}$ from the other terms in (5) (resp. (6)).
Stage 2: Assuming that $\zeta \approx \bar{\zeta}$, the Fourier coefficients of the periodic perturbation in (5) (resp. (6)) are estimated via standard parameter estimation techniques with the parametric model

$$\zeta = \Phi(\theta_m, \omega_m, \alpha_m)^\top \vartheta$$

Stage 3: Using the estimated parameters $\widehat{\vartheta}$, the velocity and acceleration estimates are constructed:

$$\widehat{\omega}_r = \omega_m - \omega_m \phi(\theta_m)^\top D \widehat{\vartheta'} \tag{8}$$

$$\widehat{\alpha}_r = \alpha_m - \left[\alpha_m \phi(\theta_m)^\top D - \omega_m^2 \psi(\theta_m)^\top D^2\right] \widehat{\vartheta''} \tag{9}$$

Experimental results

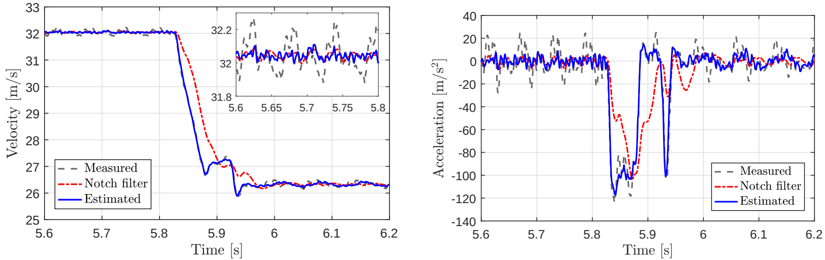

Figure: *Measured vs. filtered and estimated signals for a piecewise-constant velocity reference.*

Experimental results

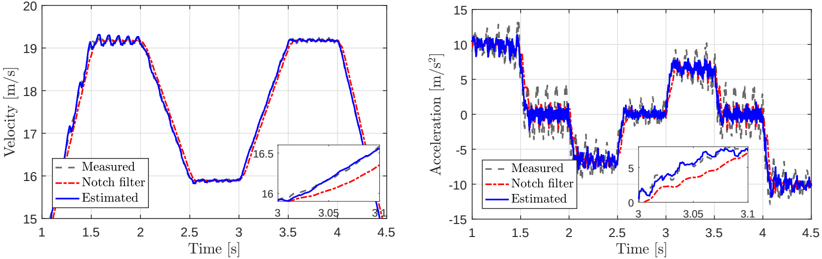

Figure: *Measured vs. filtered and estimated signals for a piecewise-linear velocity reference.*

Experimental results

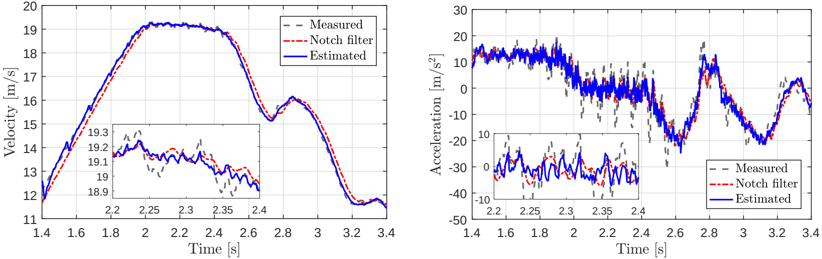

Figure: *Measured vs. filtered and estimated signals for a smooth velocity reference.*

Future work

- Joint implementation of XBS observer with estimation algorithm.
- Use of the XBS observer in closed-loop control algorithms.
- Generalization of the switched adaptive observer for a class of systems with linearizable error dynamics via singular time-scaling.
- Use of the velocity and acceleration estimation algorithm in motion control applications, e.g. electrical motors.

References

- M. Corno and S.M. Savaresi (2010). Experimental identification of engine-to-slip dynamics for traction control application in a sport motorbike. *European Journal of Control*, 16(1):88-108.
- F. Gustafsson (2010). Rotational speed sensors: limitations, pre-processing and automotive applications. IEEE Instrumentation & Measurement Magazine, 13(2):16-23.
- J.P. Hespanha (2004). Uniform stability of switched linear systems: Extensions of LaSalle's invariance principle. *IEEE Transactions on Automatic Control*, 49(4):470–482.
- T.B. Hoàng, W. Pasillas-Lépine and A. De Bernardinis (2012). Reducing the impact of wheel-frequency oscillations in continuous and hybrid ABS strategies. *Proceedings of the 11th International Symposium on Advanced Vehicle Control*.
- T.B. Hoàng, W. Pasillas-Lépine and M. Netto (2013). Closed-loop wheel-acceleration control based on an extended braking stiffness observer. *Proceedings of the American Control Conference*.
- T.B. Hoàng, W. Pasillas-Lépine, A. De Bernardinis and M. Netto (2014). Extended braking stiffness estimation based on a switched observer, with an application to wheel-acceleration control. *IEEE Transactions on Control Systems Technology*, 22(6):2384-2392.
- R. Merry, M. van de Molengraft and M. Steinbuch (2010). Velocity and acceleration estimation for optical incremental encoders. *Mechatronics*, 20(1):20-26.

References

- R. Merry, M. van de Molengraft and M. Steinbuch (2013). Optimal higher-order encoder time-stamping. *Mechatronics*, 23(5):481-490.
- G. Panzani, M. Corno and S.M. Savaresi (2012). On the periodic noise affecting wheel speed measurement. *Proceedings of the 16th IFAC Symposium on System Identification*.
- G. Rallo, S. Formentin, M. Corno, and S. M. Savaresi (2017). Real-time pedaling rate estimation via wheel speed filtering. Proceedings of the 20th IFAC World Congress, pp. 6184–6189.
- E. Ono, K. Asano, M. Sugai, S. Ito, M. Yamamoto, M. Sawada and Y. Yasui (2003). Estimation of automotive tire force characteristics using wheel velocity. *Control Engineering Practice*, 11(12):1361-1370.
- M. Sugai, H. Yamaguchi, M. Miyashita, T. Umeno and K. Asano (1999). New control technique for maximizing braking force on antilock braking system. *Vehicle System Dynamics*, 32(4-5):299-312.
- T. Umeno (2002). Estimation of tire-road friction by tire rotational vibration model. *R&D Review of Toyota CRDL*, 37(3).
- J. Villagra, B. d'Andréa Novel, M. Fliess and H. Mounier (2011). A diagnosis-based approach for tire–road forces and maximum friction estimation. *Control Engineering Practice*, 19(2):174-184.
- Q. Zhang (2002). Adaptive observer for multiple-input-multiple-output (MIMO) linear time-varying systems. *IEEE Transactions on Automatic Control*, 47(3):525-529.